Journal of Materials Chemistry A

ROYAL SOCIETY OF CHEMISTRY

COMMUNICATION

View Article Online
View Journal | View Issue

Cite this: J. Mater. Chem. A, 2025, 13, 1731

Received 30th August 2024
Accepted 25th November 2024

DOI: 10.1039/d4ta06167e

rsc.li/materials-a

A fluorinated zirconium-based metal–organic framework as a platform for the capture and removal of perfluorinated pollutants from air and water†

Daniel Hedbom, Philipp Gaiser, Tyran Günther, Ocean Cheung, Maria Strømme, Michelle Åhlén * and Martin Sjödin *

A series of zirconium-based MOFs with acclaimed stability was prepared and their ability to adsorb polyfluorinated pollutants was compared. A novel fluorinated UiO-67 analogue, named UiO-67-F_2, was synthesised alongside three previously reported materials, namely UiO-67-NH_2, UiO-68-$(CF_3)_2$, and UiO-67. The structures were established and confirmed by powder X-ray diffraction. UiO-67-NH_2, UiO-68$(CF_3)_2$ and UiO-67-F_2 were examined as sorbents for the perfluorinated gas, sulphur hexafluoride (SF_6) from the gaseous phase. The SF_6 uptake of UiO-67-NH_2 and UiO-67-F_2 at 100 kPa, 20 °C, was high (5.54 and 5.24 mmol g^{-1}, respectively). Furthermore, UiO-67-F_2 exhibited a remarkable PFOA uptake of 928 mg_{PFOA} per g_{MOF} in an aqueous solution, which far exceeded that of unmodified UiO-67 (872 mg_{PFOA} per g_{MOF} at 1000 mg_{PFOA} per L_{Water}). This study has identified strengths and potential applications of the novel UiO-67-F_2, as well as the impact of fluorine functionalization. It also offers some insight into the structure–property relations of UiO-based MOFs for their use as low-pressure SF_6 storage materials and PFAS sorbents intended for water purification under ambient conditions.

Introduction

Perfluorinated compounds encompass a large group of molecules that have found widespread use in many industrial applications and commercial products.[1] The high stability and inert nature of these molecules, stemming from the strong fluorine bonds (*e.g.*, C–F and S–F),[2,3] make them particularly challenging pollutants to remove from the environment. Per- and polyfluoroalkyl substances (PFAS) have been used since the 1940s in various applications and can be found in a wide range of products, from flame retardant foams to waterproofing agents.[4,5] In particular, fluorosurfactants (a PFAS subgroup) possess amphiphilic characteristics which enable them to reside in both water and soil.[6] Their amphiphilic nature, together with their high thermal and chemical stability, enable these compounds to persist in the environment indefinitely, thus earning them the nickname "forever chemicals"; in addition, many PFAS are toxic to living organisms.[7,8]

Other fluorinated compounds are widely used in electronic devices and the semiconductor industry as speciality gases. For instance, the low reactivity and dipole moment of sulphur hexafluoride (SF_6) make it an ideal gaseous arc suppressant.[9] Its miscibility with air and low reactivity result in SF_6 having a carbon dioxide (CO_2) equivalent of roughly 23 000 over a 100 years period, making it an extremely potent and concerning greenhouse gas.[10]

The persistent nature of perfluorinated compounds, their environmental impact, and their potential toxicity to living organisms render them highly problematic pollutants. As a result, efficient, and effective remediation strategies are necessary to safely remove and store these compounds. The removal of PFAS or SF_6 has successfully been demonstrated using techniques such as chemical oxidation, membrane filtration, and physical adsorption.[11–14] Adsorption is commonly split into two categories, one which entails a high energetic exchange and chemical binding of adsorbents (chemisorption), and one with low energetic exchange in which the formed bonds are more transient in nature (physisorption). Physisorption, using solid porous materials is a promising and effective technique, as the relatively weak bonds formed during adsorption allow for high reusability of the sorbents.

Metal–organic frameworks (MOFs), a relatively new class of porous material composed of organic ligands and inorganic metals or metal clusters, have garnered attention due to their tuneable porous structure.[15–17] The coordination bonds formed between the organic and inorganic building blocks result in durable and highly crystalline frameworks.[18] Furthermore, facile alterations or substitutions of the building blocks can be carried out pre- or post-synthetically in order to tune the adsorbate/adsorbent interaction, which is crucial when

Division of Nanotechnology and Functional Materials, Department of Materials Science and Engineering, Uppsala University, Sweden. E-mail: Michelle.Ahlen@angstrom.uu.se; Martin.Sjodin@angstrom.uu.se

† Electronic supplementary information (ESI) available. See DOI: https://doi.org/10.1039/d4ta06167e

designing a material for adsorption-based applications.[19,20] The chemical and thermal stability of a MOF is largely dependent on the bonds between the inorganic components, also known as the secondary building units (SBUs), and the organic linkers in the structure. Strong coordination bonds may be formed by combining high valence metal ions, such as Zr^{4+} and Ti^{4+}, and carboxylate-based linkers which results in the formation of robust MOF structures.[21] Zr-based MOFs, in particular the UiO-family (Universitetet i Oslo), have been shown to possess excellent thermal and chemical stability. These Zr-MOFs possess $[Zr_6O_4(OH)_4]$ cluster as its SBU which can form 12 coordination bonds with dicarboxylate-based organic linkers. The size of the voids or pore diameter of the structure can therefore be tuned by the length of the selected organic linker.[22] When comparing UiO-67 and UiO-68 derived structures (Fig. 1) containing biphenyl-4,4′-carboxylate (bpdc) and *p*-terphenyl-4,4″-dicarboxylate (tpdc) linkers, respectively, the effect can be seen as an expansion of the unit cell.[18] With perfluoro octanoic acid's (PFOA) complex adsorption mechanisms,[23] and large radius of gyration, the diameters of the hierarchical octahedral and tetrahedral pores of UiO-67 isomorphs may be more suitable than UiO-66 or 68 isomorphs. The kinetic radius of SF_6 (5.5 Å) is also expected to suit the pore diameters present in UiO-67 isomorphs, a characteristic well studied and confirmed as influential in gas adsorption.[24,25] In addition, linker fluorination as a means to improve water stability and pollutant capture has been attempted in other similar adsorbate/adsorbent pairs.[26,27]

As such, tuning of pore diameters and surface chemistry of UiO-based frameworks can be carried out by careful selection of the organic linker.

The size and chemical properties of the different functional groups may influence not only the size and shape of the cavities but also the surface chemistry. The inclusion of highly polar functional groups such as $–NH_2$ has been shown to increase the adsorption interaction with polar guest molecules or molecules possessing high quadrupole moments (*e.g.*, water and carbon dioxide).[28] The presence of electronegative atoms or groups such as $–F_2$ and $–CF_3$ may, on the other hand, change the charge distribution on the pore surface and lead to the formation of an induced electrical field gradient that can be used to increase the interaction with less polarizable molecules (*e.g.* perfluorinated adsorbates).[29,30] The host–guest interactions between UiO-67-F_2 and UiO-67, UiO-67-NH_2, UiO-68-$(CF_3)_2$ and perfluorinated guest molecules are therefore expected to differ, due to the surface chemistry and pore size of the frameworks.

In this study, we present a novel bifluorinated zirconium-based MOF, UiO-67-F_2 (Fig. 1), as a promising sorbent for the removal of perfluorinated pollutants. In the gas phase, a comparative study was conducted of SF_6 adsorbing onto UiO-67-F_2, UiO-67-NH_2, and UiO-68-$(CF_3)_2$. UiO-67-NH_2 features

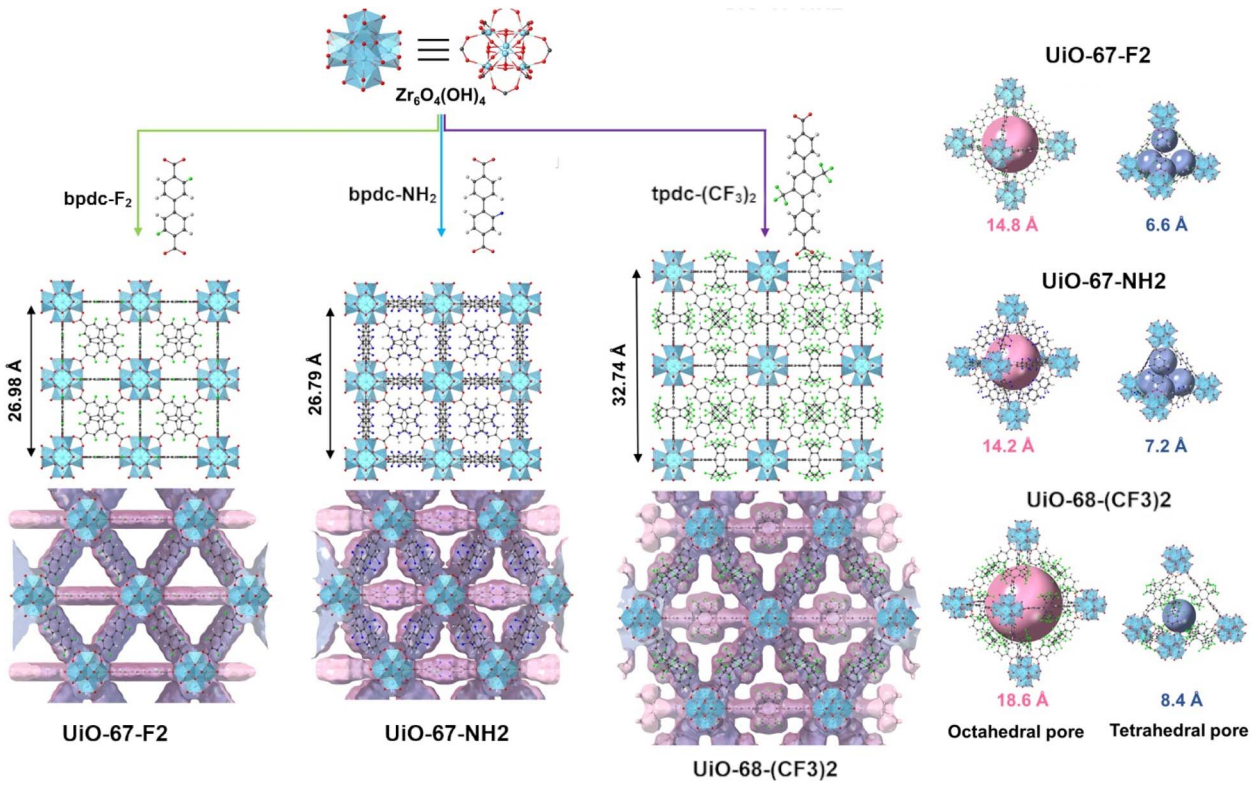

Fig. 1 Starting top left, the secondary building unit (SBU) of all UiO-MOFs, a zirconium hydroxo-cluster. This combined in three different ways with, bifluorinated biphenyl dicarboxylic acid (green, bpdc-F_2), aminated biphenyl dicarboxylic acid (blue, bpdc-NH_2) and bi-trifluoro methylated terphenyl dicarboxylic acid (purple, tpdc-$(CF_3)_2$) forming UiO-67-F_2, UiO-67-NH_2 and UiO-67-$(CF_3)_2$ respectively. UiO-67-F_2 and UiO-67-NH_2 both with similar unit cell lengths, UiO-67-$(CF_3)_2$ with much longer. All three MOFs as face centred cubic lattices with the same space group ($Fm\bar{3}m$, sg. Nr. 225). The van der Waals's surface of all three MOFs follows the same pattern, and, to the left, the octahedral and tetrahedral crystallographic pore volumes of UiO-67-F_2, UiO-67-NH_2 and UiO-67-$(CF_3)_2$ respectively.

a polar functionalization *via* an amine site, while UiO-68-$(CF_3)_2$ possesses two highly fluorinated sites. This study also considers a gradual increase in pore diameter, going from crystallographic pore sizes of 6.6–14.8 to 8.4–18.6 Å (tetrahedral–octahedral pores) in UiO-67 to UiO-68 isomorphs. From the aqueous phase, UiO-67-F_2 was also evaluated for the uptake of PFOA and its performance compared to that of unmodified, UiO-67. The primary difference between these two materials is their functionalisation, while similar pore diameters are maintained.

The structure of UiO-67-F_2, UiO-67, UiO-67-NH_2, and UiO-68-$(CF_3)_2$ MOFs (ESI, S3†) was confirmed by powder X-ray diffraction and subsequent fitting by Rietveld, and Pawley methods (ESI Section S3.1†) which showed that the compounds crystallized in the cubic $Fm\bar{3}m$ space group (No. 225).[31] The incorporation of fluorinated and aminated linkers in UiO-67-F_2 and UiO-67-NH_2, respectively, resulted in the formation of framework structures with comparable lattice parameters of a = 26.981 Å and 26.842 Å (Rietveld and Pawley fit, ESI Fig. S1–S3 and Table S1†). The structure of UiO-68-$(CF_3)_2$, containing the extended trifluoro methylated terphenyl dicarboxylate (tpdc-$(CF_3)_2$)-linker, exhibited a significantly larger lattice parameter of a = 32.849 Å (Pawley fit, ESI Fig. S1, S3 and Table S1†). Like many other MOFs in the UiO family, all three materials possess tetrahedral and octahedral cavities (Fig. 1) that arise from the interconnection between the $[Zr_6O_4(OH)_4]$ SBU and the linear dicarboxylate linkers. The diameter of the tetrahedral and octahedral cavities was found to range from approximately 6.6–8.4 Å and 14.2–18.6 Å (based on the average structure), respectively. Furthermore, the morphology of all synthesised MOFs was confirmed by scanning electron microscopy (SEM, ESI†) which showed that the materials possessed a prototypical octahedral crystal shape with a certain degree of intergrowth.[18,32,33] X-ray photoelectron spectroscopy (XPS) (ESI Fig. S5–S8†), Fourier transform infrared spectroscopy (FT-IR) (ESI Fig. S9†), scanning transmission electron microscopy (STEM), and energy-dispersive X-ray spectroscopy (EDX) were performed on UiO-67-F_2 (ESI Fig. S13–S15 and Table S10†), alongside brightfield (BF) TEM and selected-area electron diffraction (SAED) (ESI Fig S20†). The STEM-EDX (ESI S18 and S19†) and BF TEM images confirmed the elemental composition and morphology of UiO-67-F_2. High-resolution XPS spectra of the Zr 3d regions furthermore showed that the same zirconium species were present in UiO-67-F_2 as in UiO-67 and UiO-67-NH_2 which is in good agreement with the powder X-ray diffraction analysis and confirms the isoreticular structure of UiO-67-F_2. The presence of missing linker defects in UiO-67-F_2 was further assessed using thermogravimetric analysis (TGA)[34] (ESI Fig S10 and Tables S3 and S4†). The analysis suggests that UiO-67-F_2 is defective in its dehydroxylated state and has a MOF composition corresponding to $\{Zr_6O_{5.88}(C_{14}H_6F_2O_4)_{4.12}\}$ which is similar to what was seen for UiO-67-NH_2 ($\{Zr_6O_{5.87}(C_{14}H_9NO_4)_{4.13}\}$) and UiO-67 ($\{Zr_6O_{5.86}(C_{14}H_8O_4)_{4.14}\}$) (Table S4†). EDX maps of Zr and O was furthermore collected (ESI Fig. S1–S16 and Tables S4, S6–S9†) and corroborated well with the defect analysis obtained from TGA and literature. The Zr ratios to F and N in UiO-67-F_2, UiO-68-$(CF_3)_2$, and UiO-67-NH_2 were observed to be 1 : 1.4, 1 : 4.9 (original synthesis litterature[33] EDS wt% ratio at 1 : 4.7), and 1 : 1.08, respectively (compared with the theoretical Zr: F/N ratios of 1 : 2, 1 : 6, and 1 : 1).

Porosity of the materials was assessed using nitrogen (N_2) sorption isotherms recorded at −196 °C (Fig. 2(a), ESI S21–S28 and Table S11†). As expected, the Brunauer–Emmett–Teller (BET) specific surface areas (SSAs) and pore volumes were found to be comparable for UiO-67-F_2 (1966 $m^2\ g^{-1}$ and 0.781 $cm^3\ g^{-1}$), UiO-67 (2126 $m^2\ g^{-1}$ and 0.839 $cm^3\ g^{-1}$), and UiO-67-NH_2 (1883 $m^2\ g^{-1}$ and 0.750 $cm^3\ g^{-1}$) while UiO-68-$(CF_3)_2$ had a higher surface area (2911 $m^2\ g^{-1}$) and larger pore volumes (1.170 $cm^3\ g^{-1}$). The pore diameter of the structures was also observed to range from 10.0–13.5 Å in UiO-67-F_2, UiO-67, UiO-67-NH_2 and from 12.7–15.7 Å in UiO-68-$(CF_3)_2$, which agrees well with the crystallographic pore size of the respective MOFs (Fig. 1).

Sorbtive properties and selectivity of N_2, CH_4, CO_2, and SF_6 on UiO-67-F_2, UiO-67-NH_2, and UiO-68-$(CF_3)_2$ (ESI S6, Fig. S12–S16†) were assessed by gas adsorption experiments at 0, 10, and 20 °C. The magnitude of the N_2, CO_2, and CH_4 uptake were relatively low (approx. 0.2, 0.5, 1.7 mmol g^{-1} for N_2, CH_4, and CO_2 at 100 kPa, 20 °C, ESI Table S12 and Fig. S24–S26†), as expected considering the pore sizes of UiO-67-F_2, UiO-67-NH_2, and UiO-68-$(CF_3)_2$ which are too large and therefore unsuitable for the capture of small molecules (<3.8 Å in size). The corresponding selectivity by Henry's law and ideal adsorption solution theory (IAST) was calculated from single-component isotherms (ESI Fig. S29–S31 and S51–S53†) and showed that the MOFs exhibited SF_6/N_2, CO_2/N_2, CO_2/CH_4, and N_2/CH_4 selectivities below 40.

The adsorption capacity of UiO-67-F_2, UiO-67-NH_2, and UiO-68-$(CF_3)_2$ of the perfluorinated gas SF_6 was investigated. Adsorption isotherms of SF_6 collected at 20 °C and 100 kPa (Fig. 2(c)) show that the MOFs exhibit high SF_6 uptakes, ranging from 3.12 mmol g^{-1} to 5.54 mmol g^{-1} for UiO-68-$(CF_3)_2$ and UiO-67-NH_2, respectively. The SF_6 uptake of the UiO-MOFs was observed to be higher compared to other MOF structures with both lower and higher surface areas (Fig. 2(f)), such as $Cu_3(BTC)_2$ (4.43 mmol g^{-1} at 100 kPa, 25 °C, SSA 692 $m^2\ g^{-1}$, 5–13.5 Å pore size), MIL-100(Fe) (2.73 mmol g^{-1} at 100 kPa, 25 °C, SSA 1940 $m^2\ g^{-1}$, 8.7 Å pore size), UiO-66 (1.30 mmol g^{-1} at 100 kPa, 25 °C, SSA 1143 $m^2\ g^{-1}$), and UiO-67 (4.00 mmol g^{-1} at 100 kPa, 25 °C, SSA 2411 $m^2\ g^{-1}$).[16,35,43,44] This suggests that the functionalisation of the UiO-67 MOFs have a tangible effect and that pore size effects are present and significant which is evident by the large difference in SF_6 uptake at 100 kPa in UiO-67-F_2 (5.24 mmol g^{-1}) and UiO-68-$(CF_3)_2$ (3.12 mmol g^{-1}).

The calculated SF_6 occupancy at 20 °C and 100 kPa was found to be 49–63 and 49–64 molecules per unit cell and the corresponding SF_6 densities were 0.98–1.26 g L^{-1} and 1.08–1.40 g L^{-1} at 100 kPa in UiO-67-F_2 and UiO-67-NH_2, respectively. It is therefore a reasonable deduction that the measured SF_6 isotherms of UiO-67-F_2 and UiO-67-NH_2 are close to saturation at 100 kPa. As the isotherms are near saturation, we can compare their shape (Fig. 2(d and e)) to general physisorption saturation isotherms – it may be that the high uptake in UiO-67-F_2 and UiO-67-NH_2 is caused by multilayer cooperative adsorption.[45,46] This is characterized by the initial concave

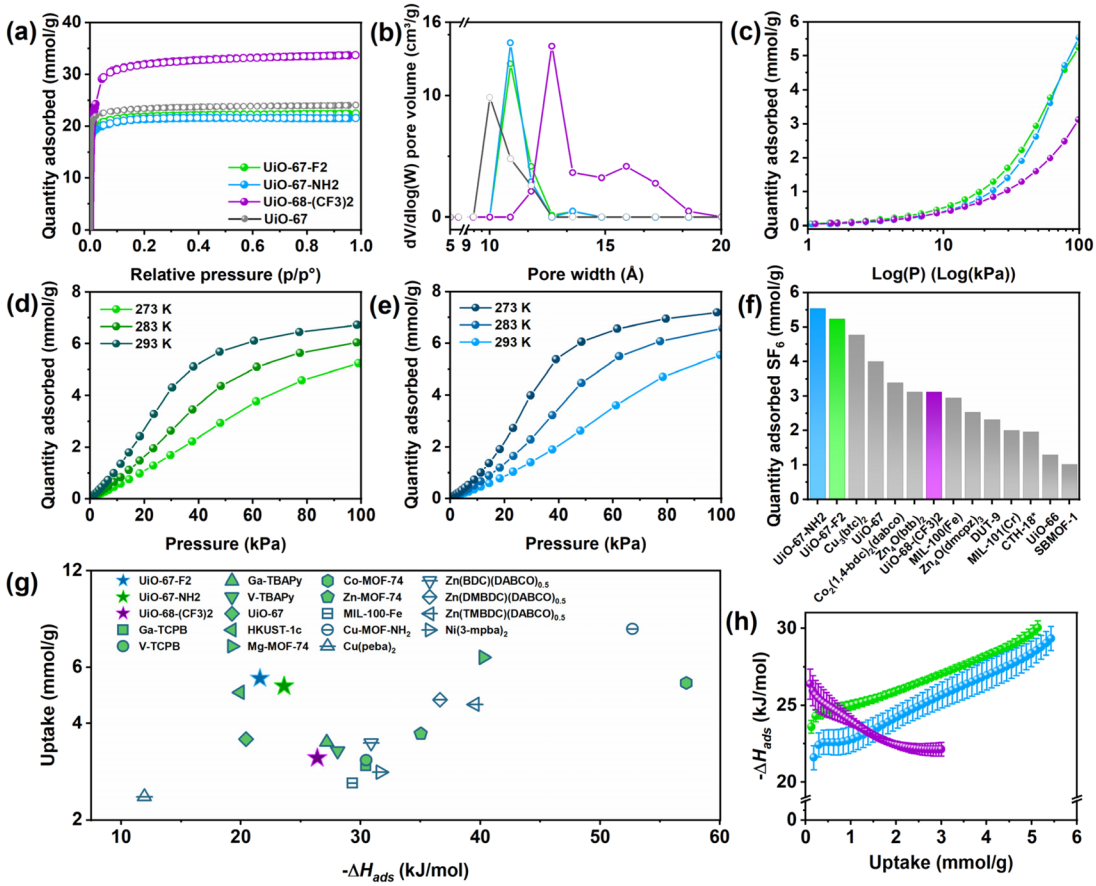

Fig. 2 (a) Nitrogen sorption isotherms recorded at -196 °C. Adsorption and desorption branches of the isotherms are depicted using filled and hollow circles, respectively. (b) DFT pore size distributions, (c) SF_6 adsorption isotherms recorded at 20 °C, (d) SF_6 adsorption isotherms for UiO-67-F_2 recorded at 0–20 °C, (e) SF_6 adsorption isotherms for UiO-67-NH_2 recorded at 0–20 °C, and (f) comparison of the SF_6 adsorption capacity at 100 kPa of various MOF sorbents, measured at 20 °C.[35–42] (g) Comparison of the SF_6 adsorption capacity at 100 kPa and enthalpies of SF_6 adsorption of various published MOF sorbents, measured at 20 °C.[35–42] (h) Isosteric enthalpies of SF_6 adsorption, error bars from each point in the linear adaptation to the isosteres.

region of the isotherm which at higher pressure becomes convex. The initially adsorbed SF_6 therefore makes it easier for subsequent SF_6 molecules to adsorb. The adsorption mechanism in UiO-68-$(CF_3)_2$ is, however, more challenging to discern as the isotherm is much further from saturation compared to the UiO-67 isomorphs.

Although the SF_6 adsorption isotherms of UiO-67-F_2 and UiO-67-NH_2 show that the materials possess superior adsorption capacities compared to UiO-68-$(CF_3)_2$ at 100 kPa. The UiO-68-$(CF_3)_2$ MOF on the other hand, has slightly higher uptake than UiO-67-NH_2 at low pressures (<9 kPa). The difference in isotherm shape (Fig. 2(c) and S50†) indicates that pore size effects are important and have a large influence over the adsorption interaction between small perfluorinated gases such as SF_6 (5.5 Å) and the framework materials in question. Although UiO-67-F_2 and UiO-67-NH_2 share many structural similarities, the presence of the polar amine or electronegative fluorine groups in their frameworks may likely influence the host–guest interactions. This effect should be most apparent at low pressures when sorbate–sorbate interactions are minimal and are observable in Fig. 2(c), where UiO-67-F_2 has a discernibly higher uptake than UiO-67-NH_2 at low–mid pressures (Fig. S50†).

SF_6 adsorption isotherms were recorded at 0–20 °C to further probe the interaction between the gas molecules and the UiO-MOF materials, Fig. 2(d, e and h). The enthalpy of adsorption ($-\Delta H_{ad}$) for the guest/host pair SF_6 and UiO-67-F_2, UiO-67-NH_2, and UiO-68-$(CF_3)_2$ was calculated according to the Clausius–Clapeyron equation and isosteric method (ESI Section S13†). UiO-67-F_2 has a higher $-\Delta H_{ads}$ (24–30 kJ mol^{-1}) than UiO-67-NH_2 (22–29 kJ mol^{-1}) between 0.12–5.13 and 0.17–5.42 mmol g^{-1} of SF_6 loading, respectively (Fig. 2(h)). Which suggests that the SF_6 molecules binds more strongly to the UiO-67-F_2 surface. Similarly, at low uptake, the more highly fluorinated UiO-68-$(CF_3)_2$ (albeit with its larger pore size) exhibits a higher $-\Delta H_{ads}$ (26 kJ mol^{-1} at 0.1 mmol g^{-1} SF_6) compared to both UiO-67-F_2 and UiO-67-NH_2. This shows that the effect of gradually increasing fluorine-functionalization (*e.g.*, from UiO-67-F_2 to UiO-68-$(CF_3)_2$) is comparatively more apparent at low pressures (~0.1–60 kPa) where interactions predominately occur between the adsorbate and adsorbent (Fig. 2(h)). As sorbate–sorbate interactions increase (with increasing pressure), pore size

effects appear more important compared to only functionalization (Fig. 2(c)). Multilayer adsorption and pore filling are adsorption events which occur at higher pressures, as we can see in Fig. 2(c). These events are more favoured in the pores of the UiO-67 isomorphs wherein an increase in $-\Delta H_{ads}$ of SF_6 is observed with pressure (Fig. 2(h)) compared to UiO-68-$(CF_3)_2$ wherein a decrease in $-\Delta H_{ads}$ can be seen in the same pressure range (Fig. 2(h)).

As shown in Fig. 2(g), UiO-67-F_2 demonstrates a very high SF_6 uptake (Fig. 2(f)) despite having a relatively low $-\Delta H_{ads}$ (24–30 kJ mol^{-1} between 0.12–5.13 mmol g^{-1} SF_6). In adsorptive gas storage applications, this characteristic is highly attractive as it may increase the efficiency of the adsorptive delivery due to the desorption of the sorbate not being enthalpically hindered by excessively favourable guest–host interactions.[47] Safety precautions in SF_6 storage furthermore necessitates dry gas mixtures, as by-products of moisture and SF_6 at high temperatures can involve HF formation. Fluorine functionalization generally makes MOFs more hydrophobic,[48] which could increase the safety of SF_6 storge in fluorine-functionalised MOFs. Therefore, an aminated sorbent like UiO-67-NH_2 would be unattractive, as amines are known hydrophiles.

In the second part of this study, UiO-67-F_2 was compared to the isoreticular and unmodified UiO-67 MOF as a sorbent for PFOA capture in aqueous solutions. As UiO-67 and UiO-67-F_2 have similar pore diameters and SSAs the functionalization of UiO-76-F_2 should be the dominant difference between the two materials. The water phase equilibrium uptake of PFOA was examined using an adapted quantitative ^{19}F-NMR method (ESI Section S17.1†), using an internal standard of trifluoroethanol (TFE). The equilibrium uptake isotherms of PFOA are shown in Fig. 3(a), wherein the fitted isotherms of UiO-67-F_2 (Langmuir maximum adsorption capacity, $q_t = 3060$ mg g^{-1}) and UiO-67 ($q_t = 1589$ mg g^{-1}) show that UiO-67-F_2 has a significantly higher PFOA adsorption capacity compared to UiO-67 (Tables S17–S20†). Compared to other published MOFs such as PCN-999 (764 mg g^{-1}, $C_0 = 1000$ mg L^{-1} PFOA), Fe-BTC (548 mg g^{-1}, $C_0 = 1000$ mg L^{-1} PFOA), and MIL-101(Cr)-QDMEN (754 mg g^{-1}, $C_0 = 1000$ mg L^{-1} PFOA) (ESI Table S21†), UiO-67-F_2 has a significantly higher uptake (928 mg g^{-1}, 1000 mg L^{-1} PFOA).[49–52] At an initial PFOA concentration of 3232 mg L^{-1}, UiO-67-F_2 has a remarkably high uptake of 1700 mg g^{-1}, which, to the best of our knowledge, is the highest reported for MOFs (Fig. 3(b) and Tables S17 and S21†).

FT-IR spectra of UiO-67-F_2 after PFOA adsorption (Fig. 3(c) and S58 ESI†) show no new bands forming as the PFOA concentration increases in samples, although some bands are red-shifted with increasing PFOA concentration. These results indicate that PFOA adsorbs onto UiO-67-F_2 without forming chemical bonds, *i.e.*, it is physically adsorbed. Furthermore, the observed dampening in band intensity between adsorbed PFOA on UiO-67 and UiO-67-F_2 differs. In similar Zr-MOFs such as NU-1000, PFOA has been observed to coordinate with free –OH sites on the SBU. In Fig. 3(d), it can be observed that the wet-state UiO-67-F_2 loses crystallinity at high PFOA uptake. This crystallinity is regained upon washing UiO-67-F_2 after adsorption Fig. 3(d). As such, the loss of crystallinity is likely due to surface/host proximity akin to that of solvent wetting, or slightly

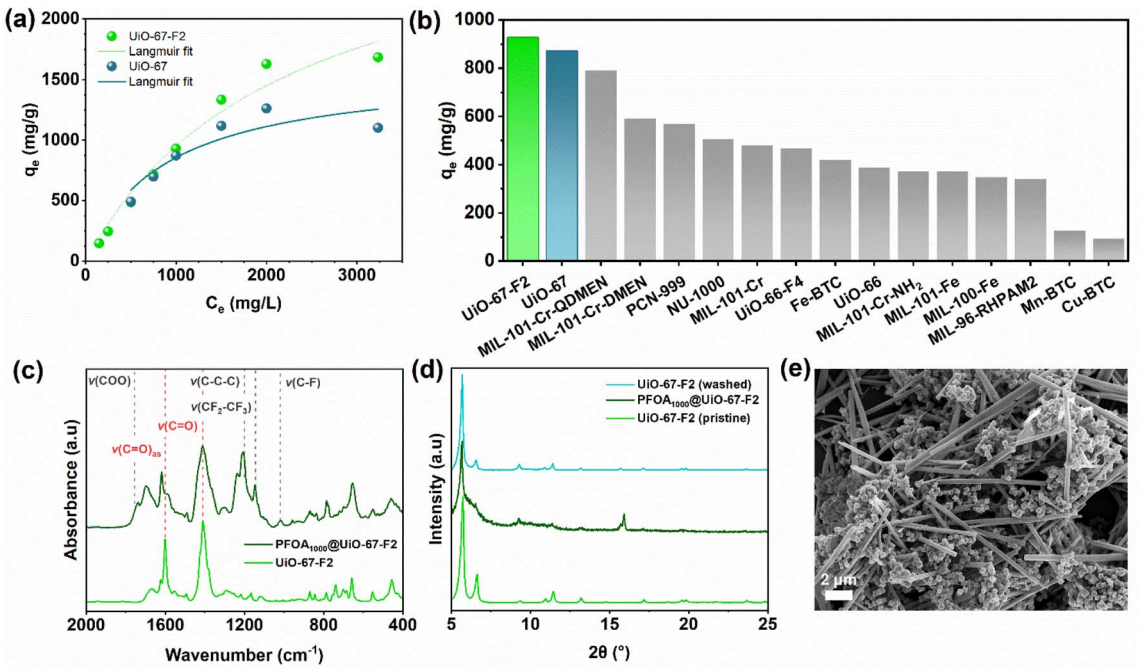

Fig. 3 (a) Equilibrium PFOA uptake of UiO-67 and UiO-67-F_2 at 25 °C after 2.5 h. Dots represent datapoints and line represents Langmuir fit, (b) PFOA uptake of various MOF sorbents at an initial PFOA concentration of 1000 mg L^{-1}, (c) FTIR spectra of pristine UiO-67-F_2 and the MOF after PFOA adsorption ($C_0 = 1000$ mg L^{-1}), dashed grey lines correspond to bands from PFOA and dashed red lines to bands from pristine UiO-67-F_2, (d) stacked normalised PXRD patterns of pristine UiO-67-F_2 and the MOF after PFOA adsorption ($C_0 = 1000$ mg L^{-1}) and after washing, and (e) SEM image UiO-67-F_2 after PFOA adsorption ($C_0 = 3232$ mg L^{-1}). Needle like structures are PFOA, octagonal crystals remain UiO-67-F_2.

flexible/dynamic host behaviour such as observed in UiO-66.[53] The SEM image in Fig. 3e shows a UiO-67-F_2 sample where the water was evaporated after exposing the MOF to 3232 mg L^{-1} PFOA (ESI Fig. S60 and S61†). From Fig. 3(d and e), we can deduce that UiO-67-F_2 does not lose its morphology upon PFOA-uptake and that the framework retains its crystallinity. The remaining PFOA in solution furthermore can be seen to precipitates into a needle-like particles when dried. All UiO isomorphs was observed to remain stable and retain their porosities after exposure to water (Fig. S7 and Table S5†) and therefore rendering them as promising sorbents for PFOA capture in aqueous solutions.

Conclusions

In summary, we have synthesised a novel MOF, UiO-67-F_2 alongside three other MOFs from published literature (UiO-67, 67-NH_2, and 68-$(CF_3)_2$). These materials were chosen for study to assess the effects that functionalization and pore-size/diameter may have on sorbtive properties of UiO-MOFs and SF_6 in gas phase or PFOA in aqueous solution. After confirming the structure and isoreticular expansion of these MOFs, it was discovered that UiO-67-F_2 may be a promising sorbent for SF_6 storage. UiO-67-F_2 was found to (1) boast a high SF_6 uptake (5.24 mmol g^{-1} at 100 kPa, 20 °C), (2) exhibit a high thermal and chemical stability, similar to other UiO-materials, and (3) have a suitable $-\Delta H_{ads}$ for ambient storage (a mean of 26.7 kJ mol^{-1} between ~0.1–5.2 mmol per g SF_6 loading). UiO-67-F_2 was also found to be a promising adsorbent for the capture and removal of PFOA in water. The fluorinated UiO-67 analogue displayed a remarkably high equilibrium PFOA uptake of 928 mg g^{-1} and 1700 mg g^{-1} at an initial PFOA concentration of 1000 and 3200 mg L^{-1}, respectively. The adsorption was found to be physisorptive and UiO-67-F_2 could be recycles after adsorption into its original state. We believe that UiO-67-F_2 may be a highly efficient PFOA-sorbent for use in water.

Data availability

The data supporting this article have been included as part of the ESI.† Crystallographic data for UiO-67-F2 has been deposited at the CCDC under deposition number 2370228 and can be obtained from DOI: **10.5517/ccdc.csd.cc2kkdzj**.

Author contributions

Daniel Hedbom, conceptualization, data curation investigation, writing – original draft, writing – review & editing, visualization, formal analysis. Philipp Gaiser, NMR-data curation, conceptualization, NMR-investigation, writing – review & editing. Tyran Günther, NMR-investigation, NMR-data curation, writing – review & editing. Michelle Åhlén, conceptualization, writing – review & editing, visualization, validation. Ocean Cheung, conceptualization, funding acquisition, writing – review & editing, resources. Maria Strømme, writing – review & editing, project administration, resources. Martin Sjödin, supervision, writing – review & editing, project administration, methodology, resources.

Conflicts of interest

There are no conflicts of interest to declare.

Acknowledgements

We acknowledge the contribution of Dr Ken Inge at Stockholm University, for his assistance in gathering capillary PXRD-data. This project received funding from the Swedish Foundation for Strategic Environmental Research (Mistra) (project name: Mistra TerraClean, project number 2015/31), the Swedish Research Council for Sustainable Development (FORMAS) (2018-00651), the Swedish Research Council (2020-04029), Stiftelsen Åforsk (19-549), and the Knut and Alice Wallenberg Foundation (2020.0033). We also acknowledge Myfab Uppsala for providing facilities and experimental support. Myfab is funded by the Swedish Research Council (2020-00207) as a national research infrastructure.

References

1 S. Y. Wee and A. Z. Aris, *npj Clean Water*, 2023, **6**, 57.
2 D. O'Hagan, *Chem. Soc. Rev.*, 2008, **37**, 308–319.
3 H. L. Roberts, *Q. Rev., Chem. Soc.*, 1961, **15**, 30.
4 C. Lau, in *Toxicological Effects of Perfluoroalkyl and Polyfluoroalkyl Substances*, ed. J. C. DeWitt, Springer International Publishing, Cham, 2015, pp. 1–21.
5 S. Y. Wee and A. Z. Aris, *npj Clean Water*, 2023, **6**, 57.
6 Y. Wang, U. Munir and Q. Huang, *Soil Environ. Health*, 2023, **1**, 100004.
7 M. Sadia, I. Nollen, R. Helmus, T. L. ter Laak, F. Béen, A. Praetorius and A. P. van Wezel, *Environ. Sci. Technol.*, 2023, **57**, 3062–3074.
8 S. E. Fenton, A. Ducatman, A. Boobis, J. C. DeWitt, C. Lau, C. Ng, J. S. Smith and S. M. Roberts, *Environ. Toxicol. Chem.*, 2021, **40**, 606–630.
9 N. Malik and A. Qureshi, *IEEE Trans. Electr. Insul.*, 1979, **EI-14**, 70–76.
10 P. Forster, V. Ramaswamy, P. Artaxo, T. Berntsen, R. Betts, D. W. Fahey, J. Haywood, J. Lean, D. C. Lowe, G. Myhre, J. Nganga, R. Prinn, G. Raga, M. Schultz and D. R. Van, *Climate Change 2007: the Physical Science Basis. Contribution of Working Group I to the Fourth Assessment Report of the Intergovernmental Panel on Climate Change*, Cambridge University Press, 2007, vol. 59.
11 X. Dai, Z. Xie, B. Dorian, S. Gray and J. Zhang, *Environ. Sci.*, 2019, **5**, 1897–1907.
12 P. M. Dombrowski, P. Kakarla, W. Caldicott, Y. Chin, V. Sadeghi, D. Bogdan, F. Barajas-Rodriguez and S. Chiang, *Remed. J.*, 2018, **28**, 135–150.
13 C. Y. Chuah, Y. Lee and T.-H. Bae, *Chem. Eng. J.*, 2021, **404**, 126577.
14 E. Gagliano, M. Sgroi, P. P. Falciglia, F. G. A. Vagliasindi and P. Roccaro, *Water Res.*, 2020, **171**, 115381.

15 M. Sai Bhargava Reddy, D. Ponnamma, K. K. Sadasivuni, B. Kumar and A. M. Abdullah, *RSC Adv.*, 2021, **11**, 12658–12681.
16 I. Senkovska, E. Barea, J. A. R. Navarro and S. Kaskel, *Microporous Mesoporous Mater.*, 2012, **156**, 115–120.
17 M. Safaei, M. M. Foroughi, N. Ebrahimpoor, S. Jahani, A. Omidi and M. Khatami, *TrAC, Trends Anal. Chem.*, 2019, **118**, 401–425.
18 J. H. Cavka, S. Jakobsen, U. Olsbye, N. Guillou, C. Lamberti, S. Bordiga and K. P. Lillerud, *J. Am. Chem. Soc.*, 2008, **130**, 13850–13851.
19 M. Åhlén, E. Kapaca, D. Hedbom, T. Willhammar, M. Strømme and O. Cheung, *Microporous Mesoporous Mater.*, 2022, **329**, 111548.
20 M. Åhlén, F. M. Amombo Noa, L. Öhrström, D. Hedbom, M. Strømme and O. Cheung, *Microporous Mesoporous Mater.*, 2022, **343**, 112161.
21 Y. An, X. Lv, W. Jiang, L. Wang, Y. Shi, X. Hang and H. Pang, *Green Chem. Eng.*, 2024, **5**, 187–204.
22 S. M. J. Rogge, J. Wieme, L. Vanduyfhuys, S. Vandenbrande, G. Maurin, T. Verstraelen, M. Waroquier and V. Van Speybroeck, *Chem. Mater.*, 2016, **28**, 5721–5732.
23 Z. Zhu, J. Duan and S. Chen, *Small*, 2024, **20**(20), 2309119.
24 M. Åhlén, A. Jaworski, M. Strømme and O. Cheung, *Chem. Eng. J.*, 2021, **422**, 130117.
25 B. Ghalei, K. Wakimoto, C. Y. Wu, A. P. Isfahani, T. Yamamoto, K. Sakurai, M. Higuchi, B. K. Chang, S. Kitagawa and E. Sivaniah, *Angew. Chem., Int. Ed.*, 2019, **58**, 19034–19040.
26 S.-Y. Ma, J. Wang, L. Fan, H.-L. Duan and Z.-Q. Zhang, *J. Chromatogr. A*, 2020, **1611**, 460616.
27 D. Balestri, I. Bassanetti, S. Canossa, C. Gazzurelli, A. Bacchi, S. Bracco, A. Comotti and P. Pelagatti, *Cryst. Growth Des.*, 2018, **18**, 6824–6832.
28 J.-R. Li, R. J. Kuppler and H.-C. Zhou, *Chem. Soc. Rev.*, 2009, **38**, 1477.
29 X.-J. Xie, H. Zeng, W. Lu and D. Li, *J. Mater. Chem. A*, 2023, **11**, 20459–20469.
30 W. Zhang, Y. Li, S. Wang, Y. Wu, S. Chen, Y. Fu, W. Ma, Z. Zhang and H. Ma, *ACS Appl. Mater. Interfaces*, 2022, **14**, 35126–35137.
31 H. M. Rietveld, *J. Appl. Crystallogr.*, 1969, **2**, 65–71.
32 N. Ko, J. Hong, S. Sung, K. E. Cordova, H. J. Park, J. K. Yang and J. Kim, *Dalton Trans.*, 2015, **44**, 2047–2051.
33 H. Wang, L. Yu, Y. Lin, J. Peng, S. J. Teat, L. J. Williams and J. Li, *Inorg. Chem.*, 2020, **59**, 4167–4171.
34 G. C. Shearer, S. Chavan, S. Bordiga, S. Svelle, U. Olsbye and K. P. Lillerud, *Chem. Mater.*, 2016, **28**, 3749–3761.
35 M. B. Kim, T. H. Kim, T. U. Yoon, J. H. Kang, J. H. Kim and Y. S. Bae, *J. Ind. Eng. Chem.*, 2020, **84**, 179–184.
36 M. Åhlén, Y. Zhou, D. Hedbom, H. S. Cho, M. Strømme, O. Terasaki and O. Cheung, *J. Mater. Chem. A*, 2023, **11**, 26435–26441.
37 C. Y. Chuah, K. Goh and T.-H. Bae, *J. Phys. Chem. C*, 2017, **121**, 6748–6755.
38 M.-B. Kim, S.-J. Lee, C. Y. Lee and Y.-S. Bae, *Microporous Mesoporous Mater.*, 2014, **190**, 356–361.
39 M.-B. Kim, T.-U. Yoon, D.-Y. Hong, S.-Y. Kim, S.-J. Lee, S.-I. Kim, S.-K. Lee, J.-S. Chang and Y.-S. Bae, *Chem. Eng. J.*, 2015, **276**, 315–321.
40 J. Ren, M. Chang, W. Zeng, Y. Xia, D. Liu, G. Maurin and Q. Yang, *Chem. Mater.*, 2021, **33**, 5108–5114.
41 S. Wang, X. Mu, H. Liu, S. Zheng and Q. Yang, *Angew. Chem., Int. Ed.*, 2022, **61**(33), e202207066.
42 L. Yan, H.-T. Zheng, L. Song, Z.-W. Wei, J.-J. Jiang and C.-Y. Su, *Chem. Eng. J.*, 2023, **472**, 145145.
43 S. S.-Y. Chui, S. M.-F. Lo, J. P. H. Charmant, A. G. Orpen and I. D. Williams, *Science*, 1999, **283**, 1148–1150.
44 L. Han, H. Qi, D. Zhang, G. Ye, W. Zhou, C. Hou, W. Xu and Y. Sun, *New J. Chem.*, 2017, **41**, 13504–13509.
45 S. Liu, *J. Colloid Interface Sci.*, 2015, **450**, 224–238.
46 K. S. W. Sing, *Pure Appl. Chem.*, 1985, **57**, 603–619.
47 S. K. Bhatia and A. L. Myers, *Langmuir*, 2006, **22**, 1688–1700.
48 L. Xie, M. Xu, X. Liu, M. Zhao and J. Li, *Adv. Sci.*, 2020, **7**(4), 1901758.
49 R.-R. Liang, S. Xu, Z. Han, Y. Yang, K.-Y. Wang, Z. Huang, J. Rushlow, P. Cai, P. Samorì and H.-C. Zhou, *J. Am. Chem. Soc.*, 2024, **146**, 9811–9818.
50 R. Li, N. N. Adarsh, H. Lu and M. Wriedt, *Matter*, 2022, **5**, 3161–3193.
51 Y. Yang, Z. Zheng, W. Ji, J. Xu and X. Zhang, *J. Hazard. Mater.*, 2020, **395**, 122686.
52 K. Liu, S. Zhang, X. Hu, K. Zhang, A. Roy and G. Yu, *Environ. Sci. Technol.*, 2015, **49**, 8657–8665.
53 K. Fabrizio, A. B. Andreeva, K. Kadota, A. J. Morris and C. K. Brozek, *Chem. Commun.*, 2023, **59**, 1309–1312.